analytical chemistry

pubs.acs.org/ac Article

Highly Sensitive and Diversified Electrochemiluminescence DNA Methylation Biosensing Platform Based on Self-Assembly of Nanotags

Xu Cao, Chen Yuan, Qian Yu, Jie Wu,* and Huangxian Ju

Cite This: *Anal. Chem.* 2025, 97, 9920−9926 Read Online

ACCESS | Metrics & More | Article Recommendations | Supporting Information

ABSTRACT: This work proposes a highly sensitive, simple, and reliable electrochemiluminescence (ECL) DNA methylation biosensing platform by employing DNA-functionalized magnetic beads (DNA-MBs) for target capture and nanotag self-assembly aggregation for signal amplification. The target methylated DNA was first captured on DNA-MBs through base pairing recognition, and then its methylation sites were recognized by antibody-5mC (Ab-5mC). Afterward, a pair of antibodies functionalized $[Ru(byp)_3]^{2+}$-doped silica nanoparticles (Ab_2-Ru@SiO_2 and Ab_3-Ru@SiO_2) was layer-by-layer assembled on Ab-5mC for amplified signal transduction. The sensing beads could be transferred to screen-printed carbon electrodes (SPCEs) for ECL curve detection via photomultiplier tube or to gold-coated indium tin oxide (Au/ITO) arrays for high-throughput imaging detection. As the nanotag assembly layers increased from 1 to 3, the detection sensitivities of SPCE-based curve detection and Au/ITO-based imaging detection were enhanced 7-fold and 3-fold, achieving detection limits down to 0.8 pM and 0.9 fM, respectively. The nanotags showed good stability, with storage times of 300 days for Ru@SiO_2 and 60 days for Ab-Ru@SiO_2, respectively. This method is universal and could be applied to detect different methylated DNAs by using their corresponding DNA-MBs. The proposed ECL biosensing platform possessed advantages of high sensitivity, good diversity, and practicality, showing potential for high-throughput DNA methylation detection in clinical diagnosis.

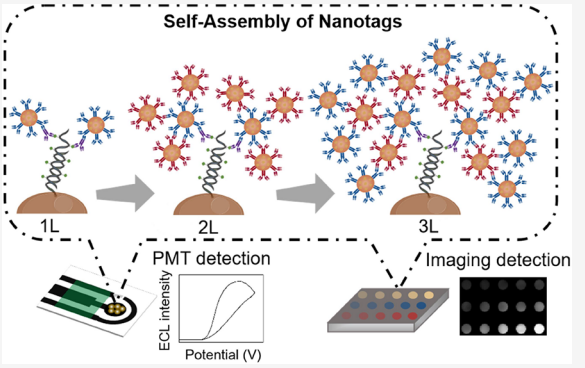

DNA methylation is a pivotal epigenetic modification that regulates gene expression without altering the DNA sequence.[1] Aberrant DNA methylation is associated with the occurrence of various diseases, such as glioblastoma, liver cancer, lung cancer, colon cancer, autoimmune diseases, and metabolic disorders.[2−4] Therefore, the development of sensitive, simple, and reliable methods for DNA methylation detection is of great significance for the early prediction and diagnosis of various genetic and cancer diseases.

Currently, the routine detection process of DNA methylation includes a sample pretreatment step by enzymatic digestion (ED) or bisulfite conversion (BC) and a nucleic acid amplification detection step, such as polymerase chain reaction (PCR),[5,6] loop-mediated isothermal amplification,[7,8] and recombinase polymerase amplification.[9] Although these methods show high detection sensitivity, they all have some intrinsic drawbacks that limit their practical applications.[10,11] For example, the BC-based strategies, including bisulfite sequencing and methylation-specific PCR, suffer from a tedious and complex workflow, rigorous operation conditions, long test time, and low conversion efficiency.[12−15] On the other hand, the ED-based strategies, including methylation-sensitive restriction enzyme digestion and methylation-dependent restriction endonucleases digestion, suffer from the incomplete digestion-caused false positive.[6,16,17]

In order to overcome the shortcomings of the routine methods, many efforts have been made to develop direct biosensing strategies that can detect DNA methylation without any sample pretreatment and nucleic acid amplification steps.[18−21] The direct detection strategies normally adopt a DNA-antibody dual recognition with a multitag label for signal output. For example, a series of direct electrochemical biosensing platforms have been reported for convenient DNA methylation detection by using antibody-5mC (Ab-5mC) or capture DNA-modified magnetic beads for target capture and horseradish peroxidase catalysts as signal labels.[22−25] These electrochemical methods have achieved sensitive detection of DNA methylation down to the pM level without bisulfite and amplification treatments. Electrochemi-

Received: January 22, 2025
Revised: April 15, 2025
Accepted: April 22, 2025
Published: April 29, 2025

https://doi.org/10.1021/acs.analchem.5c00516
Anal. Chem. 2025, 97, 9920−9926

Scheme 1. Schematic Diagram of the Diversified ECL DNA Methylation Biosensing Platform with Self-Assembly of Nanotags on Sensing Bead after the DNA-Antibody Dual Recognition of Target

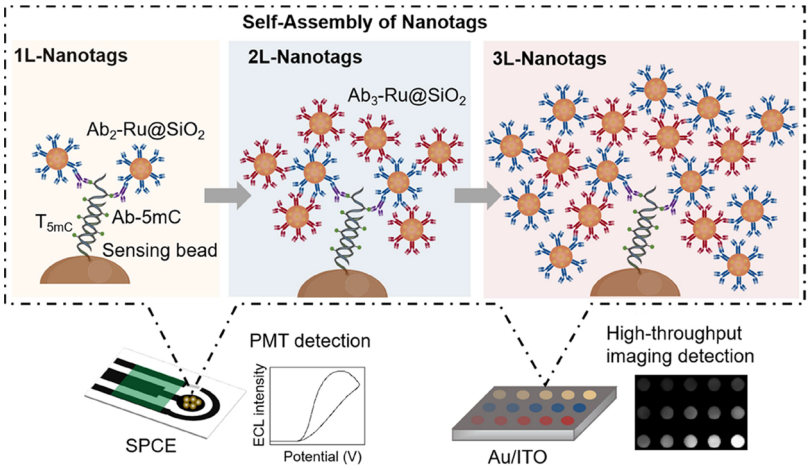

luminescence (ECL), which combines the superiorities of chemiluminescence and electrochemistry, has the advantages of low background, high sensitivity, good controllability, and simple equipment and has become one of the most advanced and widely used detection methods in clinical diagnosis and biomedical research.[26−29] Recently, our group has constructed a direct DNA methylation ECL biosensing method that uses DNA-functionalized magnetic beads (DNA-MBs) as the sensing substrate for target capture and enrichment and $[Ru(byp)_3]^{2+}$-doped silica nanoparticles ($Ru@SiO_2$) as nanotags for signal amplification.[30] Because there are over 3000 $[Ru(byp)_3]^{2+}$ in one $Ru@SiO_2$, this ECL biosensing strategy can detect the methylated DNA sequence of the promoter region of Ras-associated domain-containing protein 1 (*RASSF1A*) down to 0.5 pM. Unfortunately, in many clinical tests, this detection sensitivity is insufficient because the concentration of methylated DNA in biological samples is very low in the early stages of diseases.

The self-assembly strategy is a simple and efficient signal amplification means in biosensing.[31,32] It enhances the signal by spontaneously organizing discrete signal probes into large signal aggregates on a single biorecognition event.[33−35] A subattomolar immunoassay has been constructed by introducing the self-assembly of quantum dots into a typical sandwich-type immunoassay.[36] In addition, by introducing the self-assembly of nanoparticles into the lateral flow immunoassays, the detection sensitivity and efficiency of the strip sensors have been greatly improved.[37−41]

In this work, a highly sensitive, simple, and reliable ECL biosensing platform was proposed for methylated DNA detection by designing a nanotag self-assembly amplification on magnetic bead-based biosensing. After the DNA-antibody dual recognition of the target (T_{5mC}) on DNA-MBs, a pair of antibodies functionalized nanotags (Ab_2-$Ru@SiO_2$ and Ab_3-$Ru@SiO_2$) was layer-by-layer assembled on the biorecognition event for signal amplification. The ECL detection of methylated DNA could be achieved either by photomultiplier tube (PMT) with screen-printed carbon electrodes (SPCEs) or by camera imaging with gold-coated indium tin oxide (Au/ITO) arrays (Scheme 1). The detection sensitivity increased with the increase of assembly layers, and a sub-fM level detection limit (LOD) was achieved by the Au/ITO-based imaging detection with the three-layer assembly of nanotags (3L-Nanotags). The $Ru@SiO_2$-based nanotags could be easily synthesized with good repeatability and storage stability. This ECL biosensing platform exhibited good universality and detection diversity, showing good practicality for DNA methylation detection in the clinic.

EXPERIMENTAL SECTION

Target Sensing on Magnetic Beads with Self-Assembly of Nanotags. The materials, reagents, apparatus, and synthesis of Ab-$Ru@SiO_2$ nanotags were presented in the Supporting Information. For target sensing, DNA-MBs were first prepared similar to the previous work.[30] Briefly, 15 μL of streptavidin magnetic beads (S-MBs) were incubated with 150 μL of 0.1 μM biotin capture DNA at room temperature for 60 min, followed by a surface blocking step with 2% bovine serum albumin. After a complete washing, DNA-MBs were dispersed in 60 μL of PBST buffer and stored at 4 °C before use. The loading amount of biotin capture DNA on S-MBs was calculated to be 86 pmol mg^{-1} by UV−vis spectroscopy[42,43] (Supporting Information).

For target capture, 60 μL of DNA-MBs were mixed with 150 μL of sample solution and incubated for 30 min at 37 °C. After a centrifugation wash with PBST, the sensing beads were incubated with 150 μL of Ab-5mC (2.5 μg mL^{-1}) for 30 min at 37 °C to form DNA-MBs/T_{5mC}/Ab-5mC complexes. After another wash with PBST, 150 μL of Ab_2-$Ru@SiO_2$ (1.8 mM) was added to the sensing beads and reacted at 37 °C for 30 min to obtain 1 layer-assembly of nanotags (1L-Nanotags). These sensing beads with 1L-Nanotags were completely washed and resuspended in 150 μL of PBST for ECL detection and subsequent assembly of nanotags. Here, 100 μL of sensing beads with 1L-Nanotags were taken out and mixed with 100 μL of Ab_3-$Ru@SiO_2$ (1.8 mM) for 30 min at 37 °C to construct a 2 layer-assembly of nanotags (2L-Nanotags). After washing with centrifugation, the sensing beads with 2L-Nanotags were resuspended in 100 μL of PBST for ECL detection and the formation of 3L-Nanotags. Similarly, 50 μL of sensing beads with 2L-Nanotags was taken out and mixed with 100 μL of Ab_2-$Ru@SiO_2$ (1.8 mM) for 30 min at 37 °C to achieve 3L-Nanotags. Before ECL detection, the sensing beads with 3L-Nanotags were washed completely and dispersed in 50 μL of PBST.

https://doi.org/10.1021/acs.analchem.5c00516
Anal. Chem. 2025, 97, 9920−9926

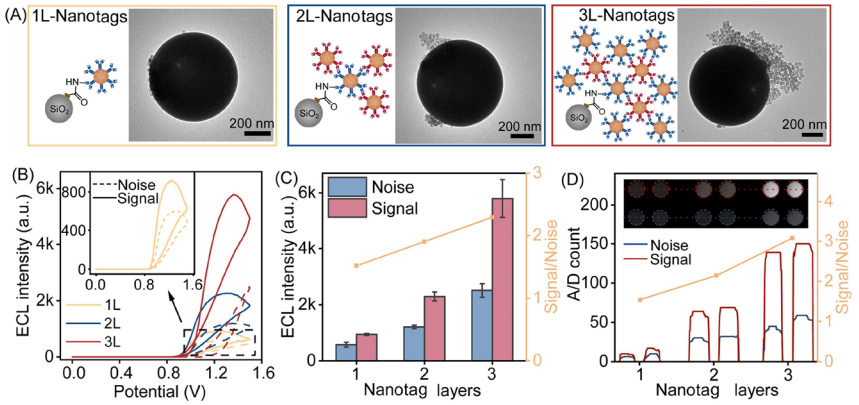

Figure 1. (A) TEM images of the self-assembly of nanotags on the surface of the COOH-SiO_2. (B) ECL curves, (C) the corresponding signal/noise ratios, and (D) ECL intensity profiles of dashed lines in ECL images of 1, 2, and 3 layer-assembly of nanotags.

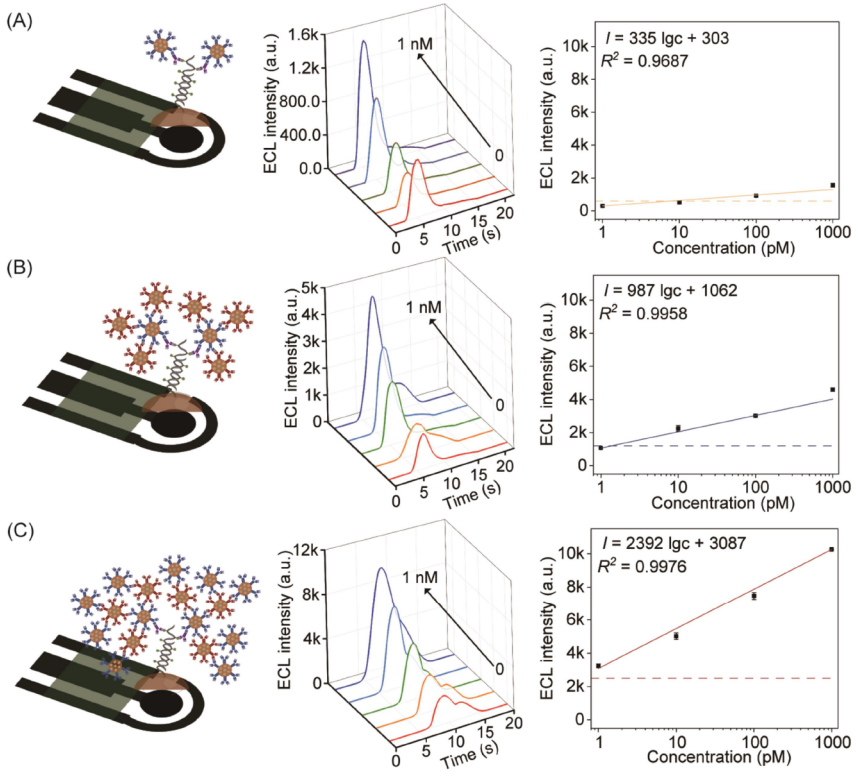

Figure 2. ECL-time curves and calibration curves of the SPCE-based detection of methylated *RASSF1A* with (A) 1L-Nanotags, (B) 2L-Nanotags, and (C) 3L-Nanotags amplification.

ECL Detection on SPCEs. 2 μL of the suspension of sensing beads with 1L-Nanotags, 2L-Nanotags, and 3L-Nanotags was dropped onto 2 mm-diameter SPCEs (Nanjing Jingjie Biotechnology Co., Ltd.), respectively. After drying, the ECL response was recorded in 0.1 M PBS (pH 7.4) containing 0.1 M KNO_3 and 40 mM tripropylamine (TPrA) at room temperature. The continuous potential scanning was performed between 0 and +1.5 V at a scanning rate of 100 mV s^{-1}, and the voltage of the PMT was set at 600 V.

ECL Imaging Detection on Au/ITO Array. The Au/ITO array was laboratory-fabricated by magnetron-sputtering 5 nm chrome and 50 nm gold on an ITO slide, followed by pasting with a porous sticker with a 3 × 6 2 mm-well design. 2.5 μL of the suspension of sensing beads with different nanotag layers was dropped onto each well of the Au/ITO array. After drying, ECL imaging with an exposure time of 31 s was conducted by continuous potential scanning from 0 to +1.5 V in 0.1 M PBS (pH 7.4) containing 0.1 M KNO_3 and 40 mM TPrA.

RESULTS AND DISCUSSION

Validation of the Nanotag Self-Assembly Amplification. This work used a pair of Ab_2-Ru@SiO_2 and Ab_3-Ru@SiO_2 nanotags to perform a layer-by-layer assembly on Ab-5mC for signal amplification. Due to the porous structure and high surface area of SiO_2 nanoparticles, Ab-Ru@SiO_2 served as an excellent signal tag, with each nanoparticle demonstrating a remarkable loading capacity of over 3000 $[Ru(bpy)_3]^{2+}$ molecules.[30] As Ab-5mC was murine antibodies, we selected antimouse IgG antibodies as Ab_2 and mouse IgG proteins as Ab_3. Thus, Ab_2-Ru@SiO_2 could not only affinity bind to Ab-5mC for first layer labeling but also bind with Ab_3-Ru@SiO_2 for subsequent self-assembly amplification. The layer-by-layer

https://doi.org/10.1021/acs.analchem.5c00516
Anal. Chem. 2025, 97, 9920−9926

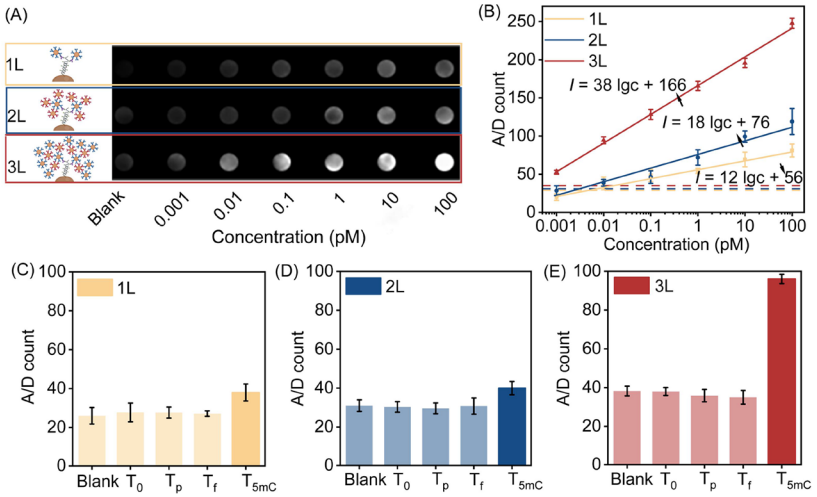

Figure 3. (A) ECL image and (B) calibration curves of imaging biosensing platforms with 1L-Nanotags, 2L-Nanotags, and 3L-Nanotags amplification. The specificity of the ECL imaging detections with (C) 1L-Nanotags, (D) 2L-Nanotags, and (E) 3L-Nanotags. The concentrations of T_{5mC}, T_0, T_P, and T_f were 10 fM, 1 pM, 1 pM, and 1 pM, respectively.

assembly of Ab_2-Ru@SiO_2 and Ab_3-Ru@SiO_2 was characterized by transmission electron microscopy (TEM), where nonmagnetic carboxylated SiO_2 (COOH-SiO_2, 700 nm in diameter) was employed to simulate the magnetic bead-based biosensing (Figure 1A). First, Ab_2-Ru@SiO_2 was covalently bound on the big COOH-SiO_2 through an amidation reaction to form a 1L-Nanotags structure. The TEM image showed that Ab_2-Ru@SiO_2 (~50 nm in diameter) existed in a single-layer form on the surface of the big COOH-SiO_2. After the reaction with Ab_3-Ru@SiO_2 to perform 2L-Nanotags, small clusters of Ab-Ru@SiO_2 were observed. By further reaction with Ab_2-Ru@SiO_2 to construct 3L-Nanotags, a large aggregation of Ab-Ru@SiO_2 was shown on the surface of the big COOH-SiO_2. These results indicated that Ab_2-Ru@SiO_2 and Ab_3-Ru@SiO_2 could be successfully assembled for aggregation amplification. The step-by-step reactions on DNA-MBs were verified by electrochemical impedance spectroscopy (Figure S1).[44] With the sequential assemblies of T_{5mC}, Ab-5mC, 1L-Nanotags, 2L-Nanotags, and 3L-Nanotags on DNA-MBs, it could be observed that the charge transfer resistance (R_{ct}) increased gradually, while the apparent charge transfer rate constant (K_{app}) decreased progressively (Table S1). This should be due to the hindrance of electron transfer caused by the progressively rising steric hindrance, verifying the detection feasibility of the proposed DNA methylation biosensing platform. In addition, the affinities of DNA-MBs toward T_{5mC} and Ab-5mC toward T_{5mC} were determined (Figure S2).[43,45] The low dissociation constants (K_d) of 2.04 and 1.86 nM indicated that T_{5mC} as well as Ab-5mC could be efficiently recognized and bound by DNA-MBs, further confirming the detection capability of this ECL biosensing platform for T_{5mC}.

The signal amplification performance of the nanotag self-assembly strategy was characterized by ECL measurements of 10 pM methylated *RASSF1A* on SPCEs (Figure 1B). The ECL curves showed that ECL intensities were progressively enhanced by the increase of nanotag assembly layers. From 1L-Nanotags to 2L-Nanotags and then to 3L-Nanotags, the signal/noise ratios increased sequentially, accompanied by a significant enhancement of the absolute signal intensity ($\Delta I = I_{singal} - I_{noise}$) (Figure 1C). The ΔI of 3L-Nanotags was 9 times that of 1L-Nanotags, indicating the effectiveness of the self-assembly strategy in signal amplification. The ECL imaging detection also showed a pronounced increase in brightness with the progression of self-assembly layers from 1 to 3 (Figure 1D). Compared to 1L-Nanotags, the 3L-Nanotags strategy exhibited a significantly high signal/noise ratio, along with a 5-fold absolute A/D count. These results confirmed the good signal amplification performance of the self-assembly of nanotags in ECL DNA methylation biosensing.

ECL Detection of Methylation DNA on SPCEs. The ECL detection was performed by transferring the sensing beads reacted with the target methylated DNA at different concentrations on SPCEs. The ECL intensities were recorded by the PMT. The results depicted in Figure 2 unveiled that the ECL intensities increased with the increase of T_{5mC} concentration in all assays with 1L-Nanotags, 2L-Nanotags, and 3L-Nanotags, and good linear relationships between ECL intensity and the logarithm of T_{5mC} concentration ranging from 1 pM to 1 nM were observed. Obviously, the detection sensitivity (the slope of the linear equation) was enhanced significantly with the increase of assembly layers. Compared to 1L-Nanotags, the sensitivities of 2L-Nanotags and 3L-Nanotags increased by 3 and 7 times, respectively. Notably, by comparing with the background, we found that the LOD of the SPCE-based ECL detection with 3L-Nanotags was decreased to 0.8 pM, while in the detections with 1L-Nanotags and 2L-Nanotags, the reliable minimum detectable concentrations were 100 and 10 pM, respectively. These results indicated that the self-assembly of nanotags could effectively enhance the detection sensitivity and improve the ECL detection performance of methylated DNA.

ECL Imaging Detection of Methylation DNA. ECL imaging detection was performed on an Au/ITO array. After the sensing beads reacted with target methylated DNA at different concentrations on their respective array wells, ECL images were obtained by a CCD camera. ECL images of the sensing beads with 1L-Nanotags, 2L-Nanotags, and 3L-Nanotags showed that the brightness of the wells gradually increased as the concentration of T_{5mC} increased from 0.001 to 100 pM (Figure 3A). The plot of ECL intensities versus the logarithm of T_{5mC} showed good linearities. The 3L-Nanotags in ECL imaging detection also exhibited the highest detection

https://doi.org/10.1021/acs.analchem.5c00516
Anal. Chem. 2025, 97, 9920−9926

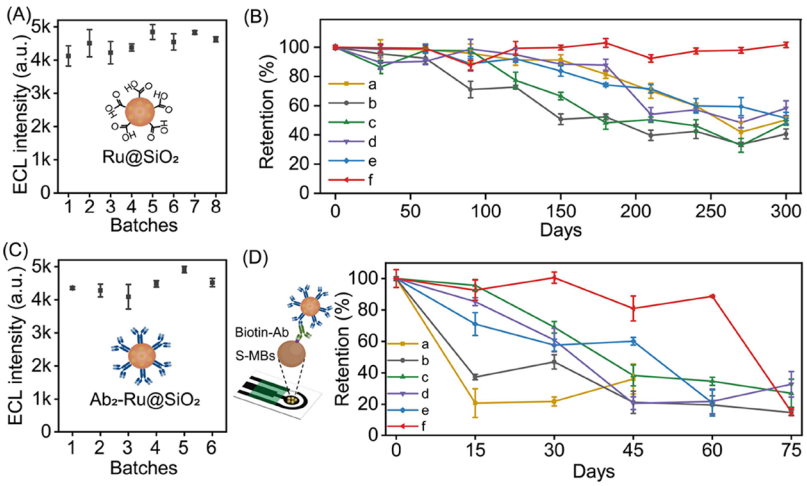

Figure 4. (A) ECL intensities of 8 batches of 2 mM Ru@SiO_2. (B) Stability of Ru@SiO_2 under 6 different conditions: (a−c) centrifugal concentration storage at −20 °C (a), 4 °C (b), room temperature (c), and (d−f) 2 mM storage at −20 °C (d), 4 °C (e), room temperature (f). (C) ECL intensities of 6 batches of 1.8 mM Ab-Ru@SiO_2. (D) Stability of Ab-Ru@SiO_2 under 6 different conditions: (a) centrifugal concentration storage at 4 °C, (b) centrifugal concentration storage at −20 °C, (c) 1.8 mM storage at 4 °C, (d) 1.8 mM storage at −20 °C, (e) 18 mM storage at 4 °C, and (f) 18 mM storage at −20 °C.

sensitivity, which was 3 and 2 times higher than those of 1L-Nanotags and 2L-Nanotags, respectively (Figure 3B). Based on the background, the LOD of ECL imaging detection with 3L-Nanotags was calculated to be 0.9 fM, which was 2 orders of magnitude lower than those of 1L-Nanotags and 2L-Nanotags. Compared with SPCE-based ECL detection, this Au/ITO-based imaging detection exhibited lower LOD, a wider detection range, better repeatability, and higher detection throughput. This might be due to the poor quality and consistency of SPCEs. In addition, when compared to previous amperometric[22−25] and ECL[30,45] DNA methylation detection methods (Table S2), the proposed ECL imaging detection with 3L-Nanotags exhibited a wide detection range with a more than 100 times lower LOD.

The specificity of the ECL imaging detection for methylated DNA was evaluated by comparing the A/D count of target methylated DNA (T_{5mC}, 7 × 5mC-*RASSF1A*) with those of other interferent DNAs at 100 times higher concentration, including an unmethylated *RASSF1A* strand (T_0), a methylated *PCDHGB7* strand (T_P), and a noncomplementary strand (T_f). Although the signal of 10 fM T_{5mC} was almost indistinguishable from those of blank and 1 pM interferent DNAs in the ECL imaging detections with 1L-Nanotags and 2L-Nanotags (Figure 3C,D), a significant signal difference between T_{5mC} and interferent DNAs was observed by ECL imaging detection with 3L-Nanotags (Figure 3E). This result indicated that the 3L-Nanotags-based ECL imaging biosensing platform possessed excellent selectivity and could effectively discern the target methylated DNA amidst a milieu of diverse sequences.

Reproducibility and Stability of the Nanotags. The present sensitive ECL DNA methylation biosensing platform was constructed based on the self-assembly of Ab-Ru@SiO_2 nanotags. Therefore, studying the reproducibility and storage stability of nanotags was crucial for evaluating the reliability and practicality of this ECL biosensing platform. We first assessed the preparation repeatability of Ru@SiO_2 by comprehensively comparing the ECL signals of 8 independent batches synthesized following identical procedures (Figure 4A). The results showed that each batch of Ru@SiO_2 exhibited consistent intensity at equivalent concentration, indicating good reproducibility of Ru@SiO_2. Then, the stability of Ru@SiO_2 was explored by placing three sets of Ru@SiO_2 under six distinct storage conditions and recording their ECL intensities every 30 days (Figure 4B). Although the ECL intensities of Ru@SiO_2 decreased significantly after 120 days in many states, the intensities of Ru@SiO_2 stored at 2 mM and room temperature remained stable, with an intensity retention of 97% after 300 days. These results demonstrated that Ru@SiO_2 possessed good reproducibility and robust long-term stability in optimal conditions, which was advantageous for the preparation of Ab-Ru@SiO_2.

Similarly, the reproducibility of Ab-Ru@SiO_2 was evaluated across 6 batches synthesized by identical procedures. The ECL intensities of these 6 batches of Ab-Ru@SiO_2 had good consistency, indicating that Ab-Ru@SiO_2 also had good preparation repeatability (Figure 4C). The stability of Ab-Ru@SiO_2 was studied by investigating its labeling activity every 15 days after storage under six different conditions. The labeling activity of Ab-Ru@SiO_2 was checked by detecting the ECL intensities of streptavidin magnetic beads (S-MBs) that were functionalized with biotin antibodies and reacted with Ab_2-Ru@SiO_2 (Figure 4D). The ECL intensities dropped sharply in most storage states, while when Ab_2−Ru@SiO_2 was stored at a high concentration (18 mM) at −20 °C, an intensity retention of 89% was achieved after 60 days. This result suggested that Ab_2-Ru@SiO_2 could maintain good labeling activity for 2 months under optimal storage conditions. The good reproducibility and stability of Ab-Ru@SiO_2 and Ru@SiO_2 ensured the practicality, durability, and longevity of the proposed ECL DNA methylation biosensing platform.

Repeatability and Universality of the ECL Imaging Biosensing Platform. To investigate the repeatability of the ECL DNA methylation biosensing platform, both the interday detection over 5 days and intraday detection over five times were conducted in the presence of 1 pM T_{5mC}.[46] The results showed desirable relative standard deviations (RSDs) of 1.14−4.30% and 3.51% in interday and intraday tests, respectively. In addition, all the $|t|_{calculated}$ values of interday (0.05−3.29, Table S3) and intraday (1.04, Table S4) tests were smaller than their

https://doi.org/10.1021/acs.analchem.5c00516
Anal. Chem. 2025, 97, 9920−9926

corresponding critical values ($|t|_{critical}$) at a $P = 0.05$, indicating exceptional repeatability with no significant systematic error of this ECL biosensing platform.

The universality of the ECL biosensing platform for DNA methylation detection was evaluated by applying the ECL imaging detection with 3L-Nanotags to detect a methylated *PCDHGB7* sequence using corresponding DNA-MBs (Figure 5A). Three parallel experiments were executed, and the results

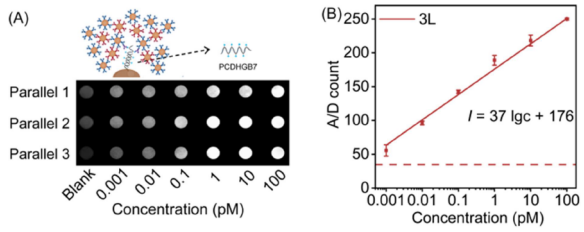

Figure 5. (A) ECL image and (B) calibration curve of detecting methylated *PCDHGB7* with 3L-Nanotags.

showed excellent repeatability. The brightness in the parallel experiments exhibited an increasing trend with the increase of target DNA concentration. The plot of ECL intensity versus the logarithm of methylated *PCDHGB7* concentration, ranging from 1 fM to 100 pM, showed good linearity (Figure 5B). The sensitivity of ECL imaging detection of methylated *PCDHGB7* was similar to that of methylated *RASSF1A*, suggesting that the present ECL biosensing platform was a stable, universal, and reliable platform for the precise detection of methylated DNA.

Real Sample Analysis. The applicability and detection performance of the ECL DNA methylation biosensing platform were assessed through recovery tests. Various concentrations of methylated *RASSF1A* were spiked into 10-fold diluted human serum samples, and the recovery rates were calculated within the range from 95 to 103% (Table S5). The RSD ranged from 1.96 to 3.03% with the $|t|_{calculated}$ (0.81−3.66) smaller than the $|t|_{critical}$ of 4.30, demonstrating the reliability and precision of the proposed ECL biosensing platform, even present in complex biological samples. The results not only underscored the versatility and accuracy of the biosensing platform but also hinted at its promising applications in clinical diagnosis.

CONCLUSIONS

This work presented a highly sensitive and diversified ECL biosensing platform for DNA methylation detection by integrating magnetic-bead-based dual recognition with a nanotag self-assembly mediated amplification strategy. This ECL biosensing platform was adaptable to diverse detection forms, including SPCE-based measurements by PMT and imaging detection on Au/ITO arrays. The self-assembly of Ab-Ru@SiO_2 nanotags enabled sensitive detection of DNA methylation, with a wide detection range of 5 orders of magnitude and a low detection limit of 0.9 fM. The platform demonstrated excellent specificity, distinguishing methylated DNA from unmethylated and noncomplementary sequences, along with high reproducibility, long-term stability, and high precision. Furthermore, the universality of the platform was validated by detecting different methylated sequences (e.g., *RASSF1A* and *PCDHGB7*) with a consistent sensitivity. This work provided a simple, robust, and ultrasensitive approach for DNA methylation detection, providing a valuable and promising means for early epigenetic testing in precision medicine.

ASSOCIATED CONTENT

Supporting Information

The Supporting Information is available free of charge at https://pubs.acs.org/doi/10.1021/acs.analchem.5c00516.

Materials and reagents; apparatus; preparation of the Ab-Ru@SiO_2 nanotags; calculation of the amount of biotin capture DNA on S-MBs; calculation of the affinities; electrochemical parameters extracted from the EIS spectra; analytical performance comparison for different kinds of electrochemical DNA methylation biosensing platforms; interday repeatability of the ECL biosensing platform; intraday repeatability of the ECL biosensing platform; recovery for detection of methylated RASSF1A in diluted serum samples; electrochemical impedance spectra of the step-by-step reaction on S-MBs; and hill plots for DNA-MBs (DOCX)

AUTHOR INFORMATION

Corresponding Author

Jie Wu − *State Key Laboratory of Analytical Chemistry for Life Science, School of Chemistry and Chemical Engineering, Nanjing University, Nanjing 210023, China;* orcid.org/0000-0003-1379-122X; Phone: +86-25-89681923; Email: wujie@nju.edu.cn

Authors

Xu Cao − *State Key Laboratory of Analytical Chemistry for Life Science, School of Chemistry and Chemical Engineering, Nanjing University, Nanjing 210023, China*

Chen Yuan − *State Key Laboratory of Analytical Chemistry for Life Science, School of Chemistry and Chemical Engineering, Nanjing University, Nanjing 210023, China*

Qian Yu − *State Key Laboratory of Analytical Chemistry for Life Science, School of Chemistry and Chemical Engineering, Nanjing University, Nanjing 210023, China*

Huangxian Ju − *State Key Laboratory of Analytical Chemistry for Life Science, School of Chemistry and Chemical Engineering, Nanjing University, Nanjing 210023, China;* orcid.org/0000-0002-6741-5302

Complete contact information is available at: https://pubs.acs.org/10.1021/acs.analchem.5c00516

Notes

The authors declare no competing financial interest.

ACKNOWLEDGMENTS

We gratefully thank the Independent Research Foundation from State Key Laboratory of Analytical Chemistry for Life Science (5431ZZXM24010) and Canon Medical Systems Corporation (2022201030) for funding supply.

REFERENCES

(1) Robertson, K. D. *Nat. Rev. Genet.* **2005**, *6*, 597−610.
(2) Roy, D.; Tiirikainen, M. *Trends Cancer* **2020**, *6*, 78−81.
(3) Zhang, H.; Liu, L.; Li, M. *ACS Sens.* **2024**, *9*, 1089−1103.
(4) Hossain, T.; Mahmudunnabi, G.; Masud, M. K.; Islam, M. N.; Ooi, L.; Konstantinov, K.; Hossain, M. S. A.; Martinac, B.; Alici, G.; Nguyen, N. T.; Shiddiky, M. J. A. *Biosens. Bioelectron.* **2017**, *94*, 63−73.

(5) Abe, M.; Kagara, N.; Miyake, T.; Tanei, T.; Naoi, Y.; Shimoda, M.; Shimazu, K.; Kim, S. J.; Noguchi, S. *Oncol. Rep.* **2019**, *42*, 2382−2389.
(6) Yang, H.; Qiu, J. N.; Zhen, L. Q.; Huang, Y. Z.; Ren, W.; Gu, H. C.; Xu, H.; Xu, G. L. *Talanta* **2022**, *247*, No. 123616.
(7) Hambalek, J. A.; Kong, J. E.; Brown, C.; Munoz, H. E.; Horn, T.; Bogumil, M.; Quick, E.; Ozcan, A.; Carlo, D. D. *ACS Sens.* **2021**, *6*, 3242−3252.
(8) An, Y. Q.; Li, Y. P.; Chen, X. L.; Han, L. R.; Xin, X. L.; Nie, H. L.; Zhang, X.; Li, C. P. *Sens. Actuators B. Chem.* **2023**, *393*, No. 134315.
(9) Wang, X. F.; Zhou, S. Y.; Chu, C. X.; Yang, M.; Huo, D. Q.; Hou, C. J. *ACS Sens.* **2021**, *6*, 2419−2428.
(10) Tan, Y. L.; Chen, H. J.; Wu, Z. K.; He, J. J.; Jiang, J. H. *Anal. Chem.* **2021**, *93*, 8077−8083.
(11) Liu, X. N.; Zhang, J. X.; Cai, Y.; Zhang, S. N.; Ma, K.; Hua, K.; Cui, Y. L. *Sens. Actuators B. Chem.* **2021**, *333*, No. 129624.
(12) Dai, Q.; Ye, C.; Irkliyenko, I.; Wang, Y. D.; Sun, H. L.; Gao, Y.; Liu, Y. S.; Beadell, A.; Perea, J.; Goel, A.; He, C. *Nat. Biotechnol.* **2024**, *42*, 1559−1570.
(13) Booth, M. J.; Ost, T. W. B.; Beraldi, D.; Bell, N. M.; Branco, M. R.; Reik, W.; Balasubramanian, S. *Nat. Protoc.* **2013**, *8*, 1841−1851.
(14) Lee, E. J.; Luo, J. F.; Wilson, J. M.; Shi, H. D. *Cancer Lett.* **2013**, *340*, 171−178.
(15) Feng, Q. M.; Wang, M. Y.; Qin, L.; Wang, P. *ACS Sens.* **2019**, *4*, 2615−2622.
(16) Liu, Y. B.; Siejka-Zielińska, P.; Velikova, G.; Bi, Y.; Yuan, F.; Tomkova, M.; Bai, C. S.; Chen, L.; Schuster-Böckler, B.; Song, C. X. *Nat. Biotechnol.* **2019**, *37*, 424−429.
(17) Pataer, P.; Zhang, P. B.; Li, Z. P. *Anal. Chem.* **2024**, *96*, 13335−13343.
(18) Bhattacharjee, R.; Moriam, S.; Nguyen, N. T.; Shiddiky, M. J. A. *Biosens. Bioelectron.* **2019**, *126*, 102−107.
(19) Huang, J.; Zhang, S.; Mo, F.; Su, S. S.; Chen, X.; Li, Y.; Fang, L. C.; Huang, H.; Deng, J.; Liu, H. M.; Yang, X. L.; Zheng, J. S. *Biosens. Bioelectron.* **2019**, *127*, 155−160.
(20) Shi, Y.; Wu, J.; Wu, W. X.; Luo, N. N.; Huang, H.; Chen, Y. H.; Sun, J.; Yu, Q.; Ao, H.; Xu, Q. Q.; Wu, X. T.; Xia, Q. F.; Ju, H. X. *Biosens. Bioelectron.* **2023**, *222*, No. 114976.
(21) Kurita, R.; Arai, K.; Nakamoto, K.; Kato, D.; Niwa, O. *Anal. Chem.* **2012**, *84*, 1799−1803.
(22) Povedano, E.; Montiel, V. R. V.; Valverde, A.; Navarro-Villoslada, F.; Yáñez-Szdeño, P.; Pedrero, M.; Montero-Calle, A.; Barderas, R.; Peláez-Carcía, A.; Mendiola, M.; Hardisson, D.; Feliú, J.; Camps, J.; Rodríguez-Tomàs, E.; Joven, J.; Arenas, M.; Campuzano, S.; Pingarrón, J. M. *ACS Sens.* **2019**, *4*, 227−234.
(23) Povedano, E.; Montiel, V. R.-V.; Gamella, M.; Pedrero, M.; Barderas, R.; Peláez-García, A.; Mendiola, M.; Hardisson, D.; Feliú, J.; Yáñez-Sedeño, P.; Campuzano, S.; Pingarrón, J. M. *Anal. Chem.* **2020**, *92*, 5604−5612.
(24) Povedano, E.; Valverde, A.; Montiel, V. R. V.; Pedrero, M.; Yáñze-Sedeño, P.; Barderas, R.; Segundo-Acosta, P. S.; Peláez-García, A.; Mendiola, M.; Hardisson, D.; Campuzano, S.; Pingarrón, J. M. *Angew. Chem., Int. Ed.* **2018**, *57*, 8194−8198.
(25) Povedano, E.; Vargas, E.; Montiel, V. R. V.; Torrente-Rodríguez, R. M.; Pedrero, M.; Barderas, R.; Segundo-Acosta, P. S.; Peláez-García, A.; Mendiola, M.; Hardisson, D.; Campuzano, S.; Pingarrón, J. M. *Sci. Rep.* **2018**, *8*, 6418.
(26) Meng, X. D.; Pang, X. J.; Yang, J. Y.; Zhang, X. J.; Dong, H. F. *Small* **2024**, *20*, No. 2307701.
(27) Barhoum, A.; Altintas, Z.; Devi, K. S. S.; Forster, R. J. *Nano Today* **2023**, *50*, No. 101874.
(28) Li, H. K.; Cai, Q. Q.; Bai, M. H.; Jie, G. F. *Anal. Chem.* **2025**, *97*, 953−961.
(29) Zhu, L.; Lv, X.; Yu, H. H.; Tan, X. R.; Rong, Y. M.; Feng, W. H.; Zhang, L. N.; Yu, J. H.; Zhang, Y. *Anal. Chem.* **2022**, *94*, 8327−8334.
(30) Wu, W. X.; Wu, J.; Huang, H.; Qian, B.; Jiang, C. L.; Shi, Y.; Wang, C.; Pei, H.; Xu, Q. Q.; Wu, X. T.; Wu, Q.; Ju, H. X. *Sens. Actuators, B* **2023**, *375*, No. 132857.
(31) Wang, Z. X.; Guo, Y. R.; Xianyu, Y. L. *Coord. Chem. Rev.* **2023**, *478*, No. 214974.
(32) Oh, H. K.; Kim, K.; Park, J.; Im, H.; Maher, S.; Kim, M. G. *Biosens. Bioelectron.* **2022**, *205*, No. 114094.
(33) Fu, C. C.; Jin, S. L.; Shi, W. B.; Oh, J.; Cao, H. Y.; Jung, Y. M. *Anal. Chem.* **2018**, *90*, 13159−13162.
(34) Men, D.; Zhang, T. T.; Hou, L. W.; Zhou, J.; Zhang, Z. P.; Shi, Y. Y.; Zhang, J. L.; Cui, Z. Q.; Deng, J. Y.; Wang, D. B.; Zhang, X. E. *ACS Nano* **2015**, *9*, 10852−10860.
(35) Gao, F. L.; Chang, Y.; Xia, N.; Li, Y. D.; Liu, L. *Microchem. J.* **2024**, *207*, No. 111921.
(36) Park, J.; Park, Y.; Kim, S. *ACS Nano* **2013**, *7*, 9416−9427.
(37) Panferov, V. G.; Ivanov, N. A.; Mazzulli, T.; Brinc, D.; Kulasingam, V.; Krylov, S. N. *Angew. Chem., Int. Ed.* **2023**, *62*, No. e202215548.
(38) Liu, S. J.; Shu, R.; Nie, C.; Li, Y. C.; Luo, X.; Ji, Y. W.; Yin, X. C.; Sun, J.; Zhang, D. H.; Wang, J. L. *Food Chem.* **2022**, *382*, No. 132390.
(39) Huang, X. L.; Zhou, Y. F.; Ding, L.; Yu, G. C.; Leng, Y. K.; Lai, W. H.; Xiong, Y. H.; Chen, X. Y. *Small* **2019**, *15*, No. 1903861.
(40) Liu, S. J.; Shu, R.; Zhang, M. R.; Zhao, C.; Wang, K. X.; Zhang, J. Y.; Sun, J.; Dou, L. N.; Zhang, D. H.; Wang, J. L. *Int. J. Biol. Macromol.* **2024**, *258*, No. 128923.
(41) Wu, Q. Y.; Yin, X. C.; Cheng, Y. Y.; Wang, C. Y.; Ma, J. Q.; Zhang, Q. Z.; Liu, H. H.; Youssef, A.; Wang, J. L.; Zhang, D. H. *Anal. Chem.* **2024**, *96*, 10714−10723.
(42) Momeni, F.; Khoshfetrat, S. M.; Zarei, K. *ACS Appl. Nano Mater.* **2023**, *6*, 19239−19248.
(43) Khoshfetrat, S. M.; Chegeni, I. *Sens. Actuators B. Chem.* **2023**, *397*, No. 134668.
(44) Mousavi, M. F.; Amiri, M.; Noori, A.; Khoshfetrat, S. M. *Electroanalysis* **2017**, *29*, 2818−2831.
(45) Khoshfetrat, S. M.; Dorraji, P. S.; Shayan, M.; Khatami, F.; Omidfar, K. *Anal. Chem.* **2022**, *94*, 8005−8013.
(46) Khoshfetrat, S. M.; Nabavi, M.; Mamivand, S.; Wang, Z.; Wang, Z.; Hosseini, M. *Microchim. Acta* **2025**, *192*, 113.

https://doi.org/10.1021/acs.analchem.5c00516
Anal. Chem. 2025, 97, 9920−9926